AIAA JOURNAL
Vol. 46, No. 5, May 2008

Aeroelastic Analysis of Wing Structures Using Equivalent Plate Models

Ranjan Vepa*
University of London, London E1 4NS, England, United Kingdom

DOI: 10.2514/1.34928

In this paper, we formulate the Reissner–Mindlin first-order shear deformation model based governing equation for a nonisotropic plate. The governing equations are cast as a set of coupled Helmholtz equations, which are then expressed as integral equations where the Green's functions are expressed in terms of the traditional Hankel functions of the first kind. The integral equations are then solved to determine the static and dynamic influence coefficients which are inverted to generate the stiffness and dynamic matrices. To demonstrate the application of these computations, we consider the aeroelastic analysis of a wing structure, modeled as an equivalent plate. The unsteady aerodynamic generalized loads are estimated by employing the doublet-lattice method, which is coupled with the compatible numerical evaluation of the structure's dynamic influence coefficient matrix, without any need for independent vibration analysis. We have demonstrated that by employing appropriate equivalent anisotropic plate models, and a variant of the classical Nyquist plot to assess the relative stability of the system, it is possible to capture, simulate, and predict all the instability features of real aircraft wings. These models are proving to be particularly useful in the synthesis of active controllers for smart structures.

Nomenclature

$\mathbf{A}$	=	coefficient matrix defined in Eq. (21)
$\mathbf{A}^0$	=	influence coefficient matrices [see Eq. (48)]
$\mathbf{B}$	=	coefficient matrix defined in Eq. (30)
$\mathbf{B}^0$	=	influence coefficient matrices [see Eq. (48)]
b	=	reference length for defining reduced frequency
C_0	=	$0.5\kappa h(\mu_1 + \mu_2)$, mean shear modulus
C_1	=	$0.5\kappa h(\mu_1 - \mu_2)$, differential shear modulus
C_{ij}	=	elastic constants relating the stresses to the strains
$\bar{C}_{ij}$	=	reduced elastic constants in Hooke's law
D	=	plate bending rigidity for an isotropic plate
$\mathbf{D}$	=	dynamic matrix in Eq. (50)
$d\mathbf{S}$	=	surface area element
E_i	=	components of the applied electric field vector
E	=	Young's modulus of an isotropic plate
E_{ij}	=	generalizations of Young's modulus
e_{ij}	=	piezoelectric constants
$\bar{e}_{ij}$	=	reduced piezoelectric constants
$\mathbf{f}$	=	external loading distribution vector
$\mathbf{G}$	=	forward path transfer function in the return difference Eq. (51)
$\mathbf{G}_i$	=	matrix of Green's functions
$\mathbf{g}$	=	control loading distribution vector
$H_0^{(1)}(z)$	=	Hankel function of the first kind and zero order
$\mathbf{H}$	=	feedback matrix in the definition of the return difference Eq. (51)
h	=	plate thickness
k_g	=	radius of gyration of plate rotary inertia per unit area, Secs. II and III
k	=	$\omega b/V$ = reduced frequency, Sec. IV
M	=	Mach number
M_{ij}	=	moment resultants across plate thickness
M_{ij}^P	=	piezoelectric or control patch moment resultants across plate thickness
$\bar{\mathbf{M}}$	=	coefficient matrix defined in Eqs. (21) and (24)
m	=	mass per unit area of the plate structure
$\mathbf{P}$	=	projection matrix defined in Eq. (36)
Q_j	=	shear force resultants across plate thickness
$\mathbf{Q}$	=	generalized aerodynamic force matrix
Q_j^P	=	piezoelectric or control patch shear force resultants across plate thickness
q	=	plate distributed loading function
q_d	=	dynamic pressure $= 0.5\rho V^2$
$\mathbf{R}_i$	=	residue matrices
s	=	rectangular wing semispan
$\mathbf{T}$	=	transformation matrix
t	=	time
$\mathbf{u}$	=	control and external loading inputs
u_i	=	three-dimensional plate displacements
u_{0i}	=	in-plane and transverse displacements of the middle surface
V	=	freestream velocity
w	=	$u_{03}(x_1, x_2)$ = transverse displacements of the plate middle surface
x_i	=	Cartesian Lagrangian coordinates
(x, y)	=	collocation or receiving point
ε_{ij}	=	plate elastic strains
ε_{ij}^0	=	reference middle surface strains
θ_i	=	rotational angles of the normal,
κ_{ij}^0	=	plate middle surface curvatures
κ	=	the Reissner–Mindlin shear correction factor
$(\lambda_i, x_i v_i)$	=	eigenvalue, right and left eigenvector triplets
μ	=	Lamé parameter
ν	=	Poisson's ratio of an isotropic plate
ν_{ij}	=	generalizations of Poisson's ratio
(ξ, η)	=	integration point or source point
σ_{ij}	=	plate elastic stresses
Φ	=	the vector of discrete values of $\{\phi_1 \quad \phi_2 \quad \phi_3\}^T$
ϕ_i	=	transformed coordinates of the plate dynamics
ω	=	circular frequency, in radians
∇^2	=	Laplacian operator

I. Introduction

STANDARD plate theory is based on the Kirchhoff assumptions that the shear deformation and rotary inertia are both zero. Thus, the Kirchhoff theory of plates is unsuitable for a variety of structures such as piezoelectric actuators, composite wing structures, as well as

Received 2 October 2007; revision received 14 January 2008; accepted for publication 16 January 2008.

*Lecturer, Department of Engineering, Queen Mary, Mile End Road; R.Vepa@qmul.ac.uk.

a number of smart structures where the shear deformation is significant or has a role to play. The shear deformation theory postulated first by Reissner [1], and extended by Mindlin [2] to include the relevant dynamics for thick plates, now known as the first-order shear deformation theory (FSDT), allows for the shear deformations and rotary inertia. It is the basis of most popular finite element implementations, such as ABAQUS. However, the finite element method (FEM) solutions, in principle, suffer from the tendency of extremely stiff modeling of bending behavior. There are indeed a number of prescribed remedies for dealing with these difficulties. One approach has been to employ an element-free Galerkin method, which possesses the important property that the nodes are not geometrically coupled by a mesh, as in the standard finite element method. If one is interested in obtaining a relatively quick solution of the structural dynamic responses to a dynamic loading, or if the interest is in modeling smart structures for control applications, the application of the FEM codes is too long-winded and tedious. On the other hand, for new structures which may be completely anisotropic, the Reissner–Mindlin theory is not too useful, as it does not simplify the governing equations a great deal, in spite of assuming a linear variation of the shear deformations across the thickness.

Many higher-order shear deformation theories (HSDT) have been proposed (Murthy [3], Phan and Reddy [4]) to partially remedy these deficiencies and shortcomings in the theory. Higher-order theories have also been proposed to model piezoelectric plate structures (Batra and Vidoli [5]). Primarily, these higher-order plate theories include additional terms in Taylor series expansion for the displacements in the three Cartesian directions in terms of generalized middle plane displacements and rotations. In the case of the simplest of these higher-order theories, this approach results in at least a cubic variation of in-plane strains ($\varepsilon_x, \varepsilon_y, \gamma_{xy}$), quadratic variation of transverse shear strains (γ_{xz}, γ_{yz}), and linear variation of transverse normal strain (ε_z) through the thickness of the plate. The HSDT is able to model both in-plane and out-of-plane modes of deformation. Phan and Reddy [4] noted that the effects of shear deformation increases significantly with material anisotropy as well as thickness. This is particularly important in the present paper because this work aims to develop a solution procedure suitable for moderately thick wings that have high material anisotropy, capable of being actuated by shape control servos. However, although the incorporation of the HSDT into the formulation will enable it to model the complex effects that arise from the actuation of the thick laminate structure, and no longer be restricted to model classical bending and twisting only, it is not expected to significantly influence the basic shape control laws or the solution procedures. Large amplitude response computations accounting for the first-order shear deformation, as well as higher-order shear deformation, may be obtained with by the FEM. The development of the nonconforming FEM does significantly reduce the computational burden significantly, while substantially avoiding the pitfalls of shear and membrane locking. Yet, there are a number of classes of orthotropic platelike structures, such as aircraft wings and piezoceramic plate actuators, that could be modeled by the Reissner–Mindlin theory. But the solution of the corresponding dynamic equations posses further difficulties, unless one resorts to a finite element approach.

In the isotropic case, the Reissner–Mindlin equations are solved by reducing the governing equations to a set of coupled Helmholtz wave equations. This reduction also permits the response to any dynamic loading to be expressed as an integral equation by employing the Green's function of the two-dimensional Helmholtz equation, which can be expressed conveniently in terms of the Hankel functions of the first kind. The Green's function approach is often the preferred approach in the solution of two- and three-dimensional airfoil and lifting surface unsteady aerodynamic flow problems, where distributions of elementary sources, doublets, and vortices are employed to construct a model for the flow dynamics. It is natural, therefore, to expect that adopting a similar approach to modeling the structure as well, would not only be consistent with the unsteady aerodynamic model, but would also be compatible with it. Thus, one could expect to model both the structural dynamic and aerodynamic operators by employing a tool such as MATLAB and obtaining the solution on a PC. However, the one drawback of such an approach would be that both the aerodynamic and structural dynamic models are no longer expressible in terms of simple polynomials of the Laplace transform variable, $s = \sigma + i\omega$ where $i = \sqrt{-1}$. The author's experience has been that this is not a very significant price to pay, and one quickly learns to use the powerful frequency domain stability analysis techniques such as the Nyquist stability criterion. Moreover, controller designs in the frequency domain are known to be very robust. Considering the modeling aspect, both the aerodynamic and structural models are "infinite" dimensional in the frequency domain, and one does not need to construct any finite state models, either to analyze the stability of the aeroelastic system or to synthesize control laws for regulation or servo control purposes.

Fiber-reinforced laminated thick/thin-walled structures are likely to play a significant role in the design of future aircraft wing structures due to their high strength and stiffness-to-weight ratios. In the case of composite, laminated thick and thin plate structures, a number of first- and higher-order theories (Demasi [6]), as well as other formulations such as the so-called zig-zag plate theories, have appeared in the literature. Introduced by Murakami [7], the zig-zag plate theories employ a zig-zag distribution of the in-plane displacements along the thickness coordinate with compatibility enforced at the interfaces. These layerwise first-order approximations give a better prediction of the transverse stresses and the in-plane displacements (Carrera [8,9]). The Reissner–Mindlin theory is still the most widely used theory for thick and anisotropic laminated plates, owing to its simplicity and its low requirement for computation capacity. For this reason, it is also being adapted to model real aircraft wings (see, for example, Kapania and Liu [10]). Aircraft wings are inherently anisotropic by construction and shear plays a major role in the deformation of these structures. When the thick plate theory is applied to such structures the anisotropy must necessarily be accounted for. It is natural that one therefore attempts to extend the solution methods available in the case of isotropic thick plates, based on the Reissner–Mindlin theory, to orthotropic and generally anisotropic situations.

In this paper, we formulate the Reissner–Mindlin first-order shear deformation model based governing equation for a nonisotropic plate. The governing equations are cast as a set of coupled Helmholtz equations, which are then partially decoupled by the application of a transformation. The equations are then expressed as integral equations where the Green's functions are expressed in terms of the traditional Hankel functions of the first kind. The integral equations are then discretized over the surface area of the wing, which is divided into a finite number of trapezoidal elemental areas or panels. The degrees of freedom are assumed to be constant over the face of each panel. The discrete integral equations are then employed to determine the static and dynamic influence coefficients which are inverted to generate the stiffness and dynamic matrices. The method shares a number of features with nonconforming finite elements.

To demonstrate the application of these computations, we consider the aeroelastic analysis of a wing structure, modeled as an equivalent plate. Our aim is to demonstrate the feasibility of modeling wing structures by equivalent plate models. There have been a few attempts in the past to analyze the aeroelastic stability of wings by the use of platelike models, although the unsteady aerodynamic load models were restricted (see, for example, Shiau and Wu [11]) to quasi-steady theories. In this paper, we adopt the doublet-lattice method to compute the unsteady aerodynamic loading. Consistent with the doublet-lattice method, the integration points are assumed to be at the forward-quarter chord point and at midspan on each panel, whereas the collocation points are assumed to be at the rear-quarter chord point. The corresponding unsteady aerodynamic generalized loads are estimated by employing the doublet-lattice method. The stability characteristics are then ascertained from the Nyquist plot. The entire analysis is performed in MATLAB without employing any finite element code or employing nodal degrees of freedom that are coupled geometrically by a mesh.

Only the open-loop case is presented in this paper. The closed-loop, actively shape-controlled case is not a simple generalization of the uncontrolled case and will therefore be presented independently.

II. First-Order Shear Deformation Theory Revisited

The first-order shear plate theory (Reissner–Mindlin theory) is adopted in the model employed here. The first-order shear deformation theory extends the kinematics of the classical plate theory by relaxing the normality restriction and allowing for arbitrary but constant rotation of transverse normals.

The displacement equations under the assumptions of FSDT can be written as

$$u_\alpha(x_1, x_2, x_3) = u_{0\alpha}(x_1, x_2) - x_3\boldsymbol{\theta}_1(x_1, x_2) \tag{1}$$

$$u_3(x_1, x_2, x_3) = u_{03}(x_1, x_2) = w(x_1, x_2) \tag{2}$$

where Greek indices run from 1 to 2, Latin indices from 1 to 3, and u_{01}, u_{02}, u_{03} are the reference middle surface displacements along Cartesian Lagrangian coordinates x_1, x_2, and x_3, respectively, with the x_3 axis perpendicular to the undeformed plate middle surface and $\boldsymbol{\theta}_1$, $\boldsymbol{\theta}_2$ are the rotational angles of the normal in the x_1-x_3, and x_2-x_3 planes, respectively, as shown in Fig. 1.

The linear strain terms with the gradients of in-plane displacements assumed to be small are given by

$$\varepsilon_{\alpha\beta} = \varepsilon^0_{\alpha\beta} - x_3\kappa^0_{\alpha\beta} \quad \text{and} \quad \varepsilon_{\alpha 3} = (u_{03,\alpha} - \boldsymbol{\theta}_\alpha)/2 = (w_{,\alpha} - \theta_\alpha)/2 \tag{3}$$

where the reference middle surface strains are $\varepsilon^0_{\alpha\beta} = (u_{0\alpha,\beta} + u_{0\beta,\alpha})/2$, whereas the bending strains are related to the Cartesian components of the plate curvatures $\kappa^0_{\alpha\beta} = (\boldsymbol{\theta}_{\alpha,\beta} + \boldsymbol{\theta}_{\beta,\alpha})/2$. The constitutive relations relate the moment resultants to the bending strains and the shear force resultants to the shear strain. These are derived from the generalized Hooke's law, which for a "special" orthotropic plate as defined by Stein et al. [12], which is also piezoelectric, is given by

$$\begin{Bmatrix} \boldsymbol{\sigma}_{11} \\ \boldsymbol{\sigma}_{22} \\ \boldsymbol{\sigma}_{33} \\ \boldsymbol{\sigma}_{23} \\ \boldsymbol{\sigma}_{31} \\ \boldsymbol{\sigma}_{12} \end{Bmatrix} = \begin{bmatrix} C_{11} & C_{12} & C_{13} & 0 & 0 & 0 \\ C_{21} & C_{22} & C_{23} & 0 & 0 & 0 \\ C_{31} & C_{32} & C_{33} & 0 & 0 & 0 \\ 0 & 0 & 0 & C_{44} & 0 & 0 \\ 0 & 0 & 0 & 0 & C_{55} & 0 \\ 0 & 0 & 0 & 0 & 0 & C_{66} \end{bmatrix} \begin{Bmatrix} \varepsilon_{11} \\ \varepsilon_{22} \\ \varepsilon_{33} \\ \varepsilon_{23} \\ \varepsilon_{31} \\ \varepsilon_{12} \end{Bmatrix} + \begin{bmatrix} 0 & 0 & e_{31} \\ 0 & 0 & e_{32} \\ 0 & 0 & e_{33} \\ 0 & e_{24} & 0 \\ e_{15} & 0 & 0 \\ 0 & 0 & 0 \end{bmatrix} \begin{Bmatrix} E_1 \\ E_2 \\ E_3 \end{Bmatrix} \tag{4}$$

where $\boldsymbol{\sigma}_{ij}$ are the stresses, ε_{ij} are the strains, C_{ij} are the elastic constants relating the stresses to the strains, e_{ij} are the piezoelectric constants, and E_i are components of the applied electric field vector.

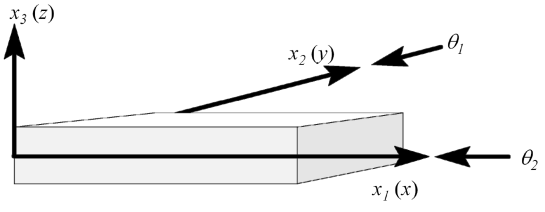

Fig. 1 Plate reference axes and the definition of the rotation angles.

In case the material is isotropic, then

$$C_{11} = C_{22} = C_{33} = \frac{E(1-\nu)}{(1+\nu)(1-2\nu)},$$
$$C_{12} = C_{13} = C_{23} = \frac{E\nu}{(1+\nu)(1-2\nu)} \quad \text{and} \tag{5}$$
$$C_{44} = C_{55} = C_{66} = \frac{E}{2(1+\nu)}$$

Here E is the Young's modulus and ν is the Poisson's ratio.

The normal stress $\boldsymbol{\sigma}_{33}$ is assumed to be *small* in comparison with other normal stresses and is neglected. Whitney and Pagano [13] have shown that, with this assumption, Eq. (4) reduces to the following contracted form:

$$\begin{Bmatrix} \boldsymbol{\sigma}_{11} \\ \boldsymbol{\sigma}_{22} \\ \boldsymbol{\sigma}_{12} \\ \boldsymbol{\sigma}_{23} \\ \boldsymbol{\sigma}_{13} \end{Bmatrix} = \begin{bmatrix} \bar{C}_{11} & \bar{C}_{12} & 0 & 0 & 0 \\ \bar{C}_{21} & \bar{C}_{22} & 0 & 0 & 0 \\ 0 & 0 & \bar{C}_{66} & 0 & 0 \\ 0 & 0 & 0 & \bar{C}_{44} & 0 \\ 0 & 0 & 0 & 0 & \bar{C}_{55} \end{bmatrix} \begin{Bmatrix} \varepsilon_{11} \\ \varepsilon_{22} \\ \varepsilon_{12} \\ \varepsilon_{23} \\ \varepsilon_{13} \end{Bmatrix} + \begin{bmatrix} 0 & 0 & \bar{e}_{31} \\ 0 & 0 & \bar{e}_{32} \\ 0 & 0 & 0 \\ 0 & \bar{e}_{24} & 0 \\ \bar{e}_{15} & 0 & 0 \end{bmatrix} \begin{Bmatrix} E_1 \\ E_2 \\ E_3 \end{Bmatrix} \tag{6}$$

where

$$\bar{C}_{ij} = C_{ij} - \frac{C_{i3}C_{3j}}{C_{33}}, \qquad \bar{e}_{ij} = e_{ij} - \frac{C_{i3}e_{3j}}{C_{33}}$$

Moments about the middle surface of the first three of these relations, when integrated across the thickness of the plate, give the moment resultant relations, whereas the last two, when integrated across the thickness of the plate, give shear force relations. For an isotropic, nonpiezoelectric plate, the moment resultants $\{M_{11} \quad M_{22} \quad M_{12}\}^T$ may be expressed in terms of plate curvatures $\kappa^0_{\alpha\beta}$ as

$$\begin{Bmatrix} M_{11} \\ M_{22} \\ M_{12} \end{Bmatrix} = D\begin{bmatrix} 1 & \nu & 0 \\ \nu & 1 & 0 \\ 0 & 0 & \frac{(1-\nu)}{2} \end{bmatrix} \begin{Bmatrix} \kappa^0_{11} \\ \kappa^0_{22} \\ 2\kappa^0_{12} \end{Bmatrix}, \qquad D = \frac{Eh}{(1-\nu^2)} \times \frac{h^2}{12} \tag{7}$$

where E is the is the Young's modulus, h is the plate thickness, and ν is the Poisson's ratio. The shear forces $\{Q_1 \quad Q_2\}^T$ may be expressed in terms of the shear strains $\varepsilon_{\alpha 3}$ as

$$\begin{Bmatrix} Q_1 \\ Q_2 \end{Bmatrix} = \kappa h \begin{bmatrix} \mu & 0 \\ 0 & \mu \end{bmatrix} \begin{Bmatrix} \varepsilon_{13} \\ \varepsilon_{23} \end{Bmatrix} \tag{8}$$

where κ is the Reissner–Mindlin shear correction factor ($=\pi^2/12$ or $5/6$) and μ is a Lamé parameter. Two different expressions may be derived for κ in the case of isotropic plates based on energy or deformation considerations. Moreover, for orthotropic materials, it is often set equal to unity.

The moment resultants must satisfy the conditions for moment equilibrium, and for a typical platelike structure, these may be expressed as

$$\frac{\partial M_{11}}{\partial x_1} + \frac{\partial M_{12}}{\partial x_2} + Q_1 = mk_g^2\frac{\partial^2\boldsymbol{\theta}_1}{\partial t^2} \tag{9}$$

$$\frac{\partial M_{12}}{\partial x_1} + \frac{\partial M_{22}}{\partial x_2} + Q_2 = mk_g^2 \frac{\partial^2 \boldsymbol{\theta}_2}{\partial t^2} \tag{10}$$

where $\boldsymbol{\theta}_1$ and $\boldsymbol{\theta}_2$ are positive section rotations about the $-x_2$ and $+x_1$ axes, respectively, m is the mass per unit area of the plate structure, and k_g is the radius of gyration of the rotary inertia of the plate per unit area. The last two quantities could vary across the surface of the plate but we shall assume for simplicity that they are constants, i.e., the inertial properties of the plate are uniform. The shear force resultants satisfy the equilibrium equation

$$\frac{\partial Q_1}{\partial x_1} + \frac{\partial Q_2}{\partial x_2} + q = m \frac{\partial^2 w}{\partial t^2} \tag{11}$$

where q is the external loading on the surface of the plate.

Inserting the constitutive relations into the equilibrium equations, the governing equations for the Reissner–Mindlin isotropic plate can be expressed in terms of the transverse displacement w and the section bending rotations $\boldsymbol{\theta}_1$ and $\boldsymbol{\theta}_2$ as

$$D\left[\frac{(1-\nu)}{2}\nabla^2\boldsymbol{\theta}_1 + \frac{(1+\nu)}{2}(\boldsymbol{\theta}_{1,11} + \boldsymbol{\theta}_{2,21})\right] + \kappa h\mu(w_{,1} - \boldsymbol{\theta}_1) = mk_g^2 \frac{\partial^2 \boldsymbol{\theta}_1}{\partial t^2} \tag{12}$$

$$D\left[\frac{(1-\nu)}{2}\nabla^2\boldsymbol{\theta}_2 + \frac{(1+\nu)}{2}(\boldsymbol{\theta}_{1,12} + \boldsymbol{\theta}_{2,22})\right] + \kappa h\mu(w_{,2} - \boldsymbol{\theta}_2) = mk_g^2 \frac{\partial^2 \boldsymbol{\theta}_2}{\partial t^2} \tag{13}$$

$$\kappa h\mu(w_{,11} + w_{,22} - \boldsymbol{\theta}_{1,1} - \boldsymbol{\theta}_{2,2}) + q = m \frac{\partial^2 w}{\partial t^2} \tag{14}$$

The exact solution of these equations was obtained by Wen and Aliabadi [14], who introduced three potential functions which satisfy three independent Helmholtz equations in two dimensions. Although there are several methods of solving the Helmholtz equation based on geometric optics, Green's functions, Fourier transforms, etc., they adopt a Fourier-transform-based method to solve them numerically.

We are now ready to consider the orthotropic case. As mentioned earlier, the general anisotropic case is best solved by considering a higher-order deformation theory and, for this reason, we do not consider the case of general anisotropy. In the orthotropic case, the constitutive relations may be expressed in a form that is easily reduced to the form presented previously for an isotropic plate when the plate is isotropic. It is assumed that the plate is not piezoelectric, but actuated by piezoelectric material or other similar patches. Thus, the relations are expressed as

$$\begin{Bmatrix} M_{11} \\ M_{22} \\ M_{12} \end{Bmatrix} = \begin{bmatrix} D_{11} & \nu_{21}D_{11} & 0 \\ \nu_{12}D_{22} & D_{22} & 0 \\ 0 & 0 & D_{33}(1-\nu_{33})/2 \end{bmatrix} \begin{Bmatrix} \kappa_{11}^0 \\ \kappa_{22}^0 \\ 2\kappa_{12}^0 \end{Bmatrix} + \begin{Bmatrix} M_{11}^P \\ M_{22}^P \\ M_{12}^P \end{Bmatrix} \tag{15a}$$

and

$$\begin{Bmatrix} Q_1 \\ Q_2 \end{Bmatrix} = \kappa h \begin{bmatrix} \mu_1 & 0 \\ 0 & \mu_2 \end{bmatrix} \begin{Bmatrix} \varepsilon_{13} \\ \varepsilon_{23} \end{Bmatrix} + \begin{Bmatrix} Q_1^P \\ Q_2^P \end{Bmatrix} \tag{15b}$$

where $\{\, M_{11}^P \quad M_{22}^P \quad M_{12}^P \,\}^T$ and $\{\, Q_1^P \quad Q_2^P \,\}^T$ are the moment and shear force resultants that appear due to the piezoelectric contributions to the stresses in the constitutive relations relating to the actuator patches. The parameter D_{33} is related to the shear modulus G_{12} and is estimated from E_{12}. The parameters E_{12} and D_{ij} are then consistently defined by

$$\begin{aligned} E_{12} &= 2G_{12}(1 - \nu_{21}\nu_{12}) + \nu_{21}E_{11} \equiv E_{33}, \\ D_{ij} &= E_{ij}h^3/12(1 - \nu_{21}\nu_{12}) \end{aligned} \tag{16}$$

The parameters ν_{21} and ν_{12} are the usual generalizations of Poisson's ratio which satisfy the relation $\nu_{12} = \nu_{21}E_{11}/E_{22}$, whereas the parameter ν_{33} is defined by $\nu_{33} = \nu_{21}E_{11}/E_{12}$.

The applied moment and shear force resultants are functions of the distance of the actuator patch from the plate middle surface, the shape function of the active area of the actuator patch, and certain actuator constants that could be derived from the constitutive relations and the transformations relating the principal directions of orthotropy of the actuator patch and the plate. These have been included so that we could derive the general equations governing an orthotropic plate externally driven by embedded piezoelectric actuator patches. The governing displacement and rotation equations now reduce to

$$\begin{aligned} &D_{33}\frac{(1-\nu_{33})}{2}\nabla^2\boldsymbol{\theta}_1 + \left(D_{11} - D_{33}\frac{(1-\nu_{33})}{2}\right)\boldsymbol{\theta}_{1,11} \\ &\quad + \left(\nu_{21}D_{11} + D_{33}\frac{(1-\nu_{33})}{2}\right)\boldsymbol{\theta}_{2,21} + \kappa h\mu_1(w_{,1} - \boldsymbol{\theta}_1) \\ &\quad + \frac{\partial M_{11}^P}{\partial x_1} + \frac{\partial M_{12}^P}{\partial x_2} = mk_g^2\frac{\partial^2\boldsymbol{\theta}_1}{\partial t^2} \end{aligned} \tag{17}$$

$$\begin{aligned} &D_{33}\frac{(1-\nu_{33})}{2}\nabla^2\boldsymbol{\theta}_2 + \left(D_{22} - D_{33}\frac{(1-\nu_{33})}{2}\right)\boldsymbol{\theta}_{2,22} \\ &\quad + \left(\nu_{12}D_{22} + D_{33}\frac{(1-\nu_{33})}{2}\right)\boldsymbol{\theta}_{1,12} + \kappa h\mu_2(w_{,2} - \boldsymbol{\theta}_2) \\ &\quad + \frac{\partial M_{12}^P}{\partial x_1} + \frac{\partial M_{22}^P}{\partial x_2} = mk_g^2\frac{\partial^2\boldsymbol{\theta}_2}{\partial t^2} \end{aligned} \tag{18}$$

$$\begin{aligned} &\kappa h\mu_1(w_{,11} - \boldsymbol{\theta}_{1,1}) + \kappa h\mu_2(w_{,22} - \theta_{2,2}) + \frac{\partial Q_1^P}{\partial x_1} + \frac{\partial Q_2^P}{\partial x_2} + q \\ &\quad = m\frac{\partial^2 w}{\partial t^2} \end{aligned} \tag{19}$$

III. Alternate Formulations of the Governing Equations

To facilitate their solution, we rewrite the preceding governing equations of motion [Eqs. (17–19)] for an orthotropic plate in a slightly different form. As our intention is to solve the preceding governing equations of motion, we first differentiate the first two equations with respect to x_1 and x_2, respectively, and add and subtract the two resulting equations, respectively. Eliminating the w terms from the first of these equations, they are then written in matrix form as

$$\begin{aligned} &\left(\begin{bmatrix} D_0 & D_1 & 0 \\ D_2 & D_4 & C_1 \\ 0 & 0 & C_0 \end{bmatrix}\nabla^2 + \begin{bmatrix} D_2 & D_3 & 0 \\ D_5 & D_1 & C_0 \\ 0 & 0 & C_1 \end{bmatrix}\left(\frac{\partial^2}{\partial x_1^2} - \frac{\partial^2}{\partial x_2^2}\right) \right. \\ &\quad \left. - \begin{bmatrix} 0 & 0 & 0 \\ C_1 & C_0 & 0 \\ C_0 & C_1 & 0 \end{bmatrix}\right)\begin{Bmatrix} \boldsymbol{\theta}_{1,1} + \boldsymbol{\theta}_{2,2} \\ \boldsymbol{\theta}_{1,1} - \boldsymbol{\theta}_{2,2} \\ w \end{Bmatrix} \\ &\quad + \begin{Bmatrix} \frac{\partial^2 M_{11}^P}{\partial x_1^2} + 2\frac{\partial^2 M_{12}^P}{\partial x_1 \partial x_2} + \frac{\partial^2 M_{22}^P}{\partial x_2^2} - \frac{\partial Q_1^P}{\partial x_1} - \frac{\partial Q_2^P}{\partial x_2} \\ \frac{\partial^2 M_{11}^P}{\partial x_1^2} - \frac{\partial^2 M_{22}^P}{\partial x_2^2} \\ \frac{\partial Q_1^P}{\partial x_1} + \frac{\partial Q_2^P}{\partial x_2} \end{Bmatrix} + \begin{Bmatrix} -1 \\ 0 \\ 1 \end{Bmatrix} q \\ &\quad = m\begin{bmatrix} k_g^2 & 0 & -1 \\ 0 & k_g^2 & 0 \\ 0 & 0 & 1 \end{bmatrix}\frac{\partial^2}{\partial t^2}\begin{Bmatrix} \boldsymbol{\theta}_{1,1} + \boldsymbol{\theta}_{2,2} \\ \boldsymbol{\theta}_{1,1} - \boldsymbol{\theta}_{2,2} \\ w \end{Bmatrix} \end{aligned} \tag{20}$$

where the constants D_i, $i = 0, 1, 2, \ldots, 5$, and C_i, $i = 0$ and 1, are defined as follows:

$$D_0 = (D_{11} + D_{22} + 2D_{33} + \nu_{12}D_{22} + \nu_{21}D_{11} - 2\nu_{33}D_{33})/4$$

$$D_1 = (D_{11} - D_{22} + \nu_{12}D_{22} - \nu_{21}D_{11})/4$$

$$D_2 = (D_{11} - D_{22} - \nu_{12}D_{22} + \nu_{21}D_{11})/4$$

$$D_3 = (D_{11} + D_{22} - 2D_{33} - \nu_{12}D_{22} - \nu_{21}D_{11} + 2\nu_{33}D_{33})/4$$

$$D_4 = (D_{11} + D_{22} - \nu_{12}D_{22} - \nu_{21}D_{11})/4$$

$$D_5 = (D_{11} + D_{22} + \nu_{12}D_{22} + \nu_{21}D_{11})/4$$

For an isotropic plate, $D_i = 0$, $i = 1$, 2, and 3, $D_0 = D$, $D_4 = D[(1-\nu)/2]$, $D_5 = D[(1+\nu)/2]$, and $C_1 = 0$, $C_0 = 0.5\kappa h(\mu_1 + \mu_2)$, and it follows that the second of the three governing equations in Eq. (20) is uncoupled from the other two.

Multiplying the equation by

$$\begin{bmatrix} D_0 & D_1 & 0 \\ D_2 & D_4 & C_1 \\ 0 & 0 & C_0 \end{bmatrix} = \frac{1}{\Delta \times C_0} \begin{bmatrix} C_0 D_4 & -C_0 D_1 & C_1 D_1 \\ -C_0 D_2 & C_0 D_0 & -C_1 D_0 \\ 0 & 0 & \Delta \end{bmatrix}$$

where $\Delta = D_0 D_4 - D_1 D_2$ the matrix equation reduces to

$$\left(\nabla^2 + \mathbf{A}\left(\frac{\partial^2}{\partial x^2} - \frac{\partial^2}{\partial y^2}\right)\right) \begin{Bmatrix} \boldsymbol{\theta}_{1,1} + \boldsymbol{\theta}_{2,2} \\ \boldsymbol{\theta}_{1,1} - \boldsymbol{\theta}_{2,2} \\ w \end{Bmatrix} + \mathbf{M}_0 \begin{Bmatrix} \boldsymbol{\theta}_{1,1} + \boldsymbol{\theta}_{2,2} \\ \boldsymbol{\theta}_{1,1} - \boldsymbol{\theta}_{2,2} \\ w \end{Bmatrix} + \mathbf{g} + \mathbf{f}q = \mathbf{M}_1 \frac{m}{C_0} \frac{\partial^2}{\partial t^2} \begin{Bmatrix} \boldsymbol{\theta}_{1,1} + \boldsymbol{\theta}_{2,2} \\ \boldsymbol{\theta}_{1,1} - \boldsymbol{\theta}_{2,2} \\ w \end{Bmatrix} \tag{21}$$

where,

$$\mathbf{A} = \begin{bmatrix} D_0 & D_1 & 0 \\ D_2 & D_4 & C_1 \\ 0 & 0 & C_0 \end{bmatrix}^{-1} \begin{bmatrix} D_2 & D_3 & 0 \\ D_5 & D_1 & C_0 \\ 0 & 0 & C_1 \end{bmatrix},$$

$$\mathbf{M}_0 = -\begin{bmatrix} D_0 & D_1 & 0 \\ D_2 & D_4 & C_1 \\ 0 & 0 & C_0 \end{bmatrix}^{-1} \begin{bmatrix} 0 & 0 & 0 \\ C_1 & C_0 & 0 \\ C_0 & C_1 & 0 \end{bmatrix}$$

$$\mathbf{g} = \begin{bmatrix} D_0 & D_1 & 0 \\ D_2 & D_4 & C_1 \\ 0 & 0 & C_0 \end{bmatrix}^{-1} \begin{Bmatrix} \frac{\partial^2 M_{11}^P}{\partial x_1^2} + 2\frac{\partial^2 M_{12}^P}{\partial x_1 \partial x_2} + \frac{\partial^2 M_{22}^P}{\partial x_2^2} - \frac{\partial Q_1^P}{\partial x_1} - \frac{\partial Q_2^P}{\partial x_2} \\ \frac{\partial^2 M_{11}^P}{\partial x_1^2} - \frac{\partial^2 M_{22}^P}{\partial x_2^2} \\ \frac{\partial Q_1^P}{\partial x_1} + \frac{\partial Q_2^P}{\partial x_2} \end{Bmatrix}$$

$$\mathbf{f} = \begin{bmatrix} D_0 & D_1 & 0 \\ D_2 & D_4 & C_1 \\ 0 & 0 & C_0 \end{bmatrix}^{-1} \begin{Bmatrix} -1 \\ 0 \\ 1 \end{Bmatrix} \quad \text{and}$$

$$\mathbf{M}_1 = \begin{bmatrix} D_0 & D_1 & 0 \\ D_2 & D_4 & C_1 \\ 0 & 0 & C_0 \end{bmatrix}^{-1} \begin{bmatrix} C_0 k_g^2 & 0 & -C_0 \\ 0 & C_0 k_g^2 & 0 \\ 0 & 0 & C_0 \end{bmatrix}$$

At this stage we may assume that the motion in the time domain is simple harmonic and this assumption results in one of the equation coefficients being frequency dependent. We now introduce a transformation of the independent variables defined by

$$\begin{Bmatrix} \boldsymbol{\theta}_{1,1} + \boldsymbol{\theta}_{2,2} \\ \boldsymbol{\theta}_{1,1} - \boldsymbol{\theta}_{2,2} \\ w \end{Bmatrix} = \mathbf{T} \begin{Bmatrix} \phi_1 \\ \phi_2 \\ \phi_3 \end{Bmatrix} \tag{22}$$

where the matrix $\mathbf{T}$ is the set of eigenvectors obtained by solving the eigenvalue problem

$$\left[\mathbf{M}_0 + \frac{m\omega^2}{C_0}\mathbf{M}_1\right]\mathbf{t}_i = \lambda_i \mathbf{t}_i$$

The matrix $\mathbf{T}$ is assumed to be nonsingular. If $\mathbf{T}$ is singular, it is assumed to be the Jordan canonical form or an identity matrix. In the case when $\omega = 0$, it may be well-nigh impossible to reduce $\mathbf{M}_0$ to a diagonal form due to existence of multiple equal eigenvalues. Thus, the matrix equation governing the plate motion [Eq. (21)] may be expressed as

$$\nabla^2 \begin{Bmatrix} \phi_1 \\ \phi_2 \\ \phi_3 \end{Bmatrix} + \bar{\mathbf{M}} \begin{Bmatrix} \phi_1 \\ \phi_2 \\ \phi_3 \end{Bmatrix} + \mathbf{T}^{-1}\mathbf{A}\mathbf{T}\left(\frac{\partial^2}{\partial x^2} - \frac{\partial^2}{\partial y^2}\right) \begin{Bmatrix} \phi_1 \\ \phi_2 \\ \phi_3 \end{Bmatrix} + \mathbf{T}^{-1}\mathbf{g} + \mathbf{T}^{-1}\mathbf{f}q = 0 \tag{23}$$

where $(x, y, z) = (x_1, x_2, x_3)$ and

$$\bar{\mathbf{M}} = \mathbf{T}^{-1}\left[\mathbf{M}_0 + \frac{m\omega^2}{C_0}\mathbf{M}_1\right]\mathbf{T} \tag{24}$$

When the last three terms on the left-hand side of the preceding matrix equation are ignored, it reduces to a set of three coupled two-dimensional Helmholtz equations.

IV. Integral Equation Formulations of the Response

To employ the Green's function for the two-dimensional Helmholtz equation, which can be expressed in terms of the Hankel function of the first kind and zero order, we may write the solutions for $\{\phi_1 \quad \phi_2 \quad \phi_3\}^T$ in Eq. (23) as integral equations over the surface area of the plate. Thus, in terms of the operator ∇^2, the integral equations are

$$\begin{Bmatrix} \phi_1 \\ \phi_2 \\ \phi_3 \end{Bmatrix} = \left(\frac{1}{\bar{\mathbf{M}} + \nabla^2}\right) \times \left[\mathbf{T}^{-1}\mathbf{A}\mathbf{T}\left(\frac{\partial^2}{\partial x^2} - \frac{\partial^2}{\partial y^2}\right) \begin{Bmatrix} \phi_1 \\ \phi_2 \\ \phi_3 \end{Bmatrix} + \mathbf{T}^{-1}\mathbf{g} + \mathbf{T}^{-1}\mathbf{f}q\right] \tag{25}$$

Let the eigenvalues (poles) of $\bar{\mathbf{M}}$ and the corresponding right and left eigenvectors be given by the triplets $(\lambda_i, x_i v_i)$, and let the right and left eigenvectors (column vectors) be scaled so that $v_i^T x_i = 1$. Note that $v_j^T x_k = 0$ for $j \neq k$. The dyadic expansion of the integral operator can be expressed as a sum of residue matrices $\mathbf{R}_i$ over first-order poles each of multiplicity m_i:

$$\mathbf{R}(\nabla^2) = \left(\frac{1}{\bar{\mathbf{M}} + \nabla^2}\right) = \sum_{i=1}^{3} \frac{\mathbf{R}_i}{(\nabla^2 + \lambda_i)^{m_i}} \tag{26}$$

where the residues $\mathbf{R}_i$ are $\mathbf{R}_i = x_i v_i^T$.

Thus, the integral Eq. (25) may be expressed as

$$\begin{Bmatrix} \phi_1(x,y) \\ \phi_2(x,y) \\ \phi_3(x,y) \end{Bmatrix} = \sum_{i=1}^{3} \mathbf{R}_i \iint_S \mathbf{G}_i \times \left\{ \left[\mathbf{T}^{-1}\mathbf{A}\mathbf{T}\left(\frac{\partial^2}{\partial \xi^2} - \frac{\partial^2}{\partial \eta^2}\right)\right] \begin{Bmatrix} \phi_1(\xi,\eta) \\ \phi_2(\xi,\eta) \\ \phi_3(\xi,\eta) \end{Bmatrix} + \mathbf{B}(\xi,\eta)\mathbf{u}(\xi,\eta) \right\} \mathrm{d}\mathbf{S} \tag{27}$$

where $\mathbf{G}_i$ is a diagonal matrix with elements

$$g_i = \frac{\sqrt{-1}}{4} H_0^{(1)}(\sqrt{\lambda_i} \times r) \tag{28}$$

when the pole multiplicity $m_i = 1$ and

$$g_i = \frac{\sqrt{-1}}{4} \frac{\mathrm{d}}{\mathrm{d}\lambda_i} H_0^{(1)}(\sqrt{\lambda_i} \times r) \tag{29}$$

when the pole multiplicity $m_i = 2$,

$$\mathbf{Bu} = \mathbf{T}^{-1}[\mathbf{g}(\xi, \eta) + \mathbf{f} q(\xi, \eta)] \tag{30}$$

The Hankel function of the first kind and zero order is $H_0^{(1)}(\sqrt{\lambda_i} \times r)$, (ξ, η) are the integration variables, and r is defined by $r = \sqrt{(x-\xi)^2 + (y-\eta)^2}$. When $\lambda_i = 0$, the Green's functions reduce to those corresponding to the Laplace operator $[-\log(r)/2\pi]$ and bi-Laplace operators $[r^2 \log(r)/8\pi)]$. It must be said that one could, in principle, add a constant to the Laplace operator's Green's function and a quadratic in r to the bi-Laplace operator's Green's function. In fact, for small values of $z = kr$, the Hankel function and its derivative, ignoring higher-order terms, may, respectively, be expressed as

$$H_0^{(1)}(z) = \frac{2i}{\pi} \log(r) \left(1 - \frac{z^2}{4}\right) + \left\{1 + \frac{2i}{\pi}\left[\log\left(\frac{k}{2}\right) + \gamma\right]\right\} - \frac{z^2}{4}\left\{1 + \frac{2i}{\pi}\left[\log\left(\frac{k}{2}\right) + \gamma - 1\right]\right\} \tag{31}$$

$$2\lambda_i \frac{\mathrm{d}}{\mathrm{d}\lambda_i} H_0^{(1)}(\sqrt{\lambda_i} \times r) = z \frac{\mathrm{d}}{\mathrm{d}z} H_0^{(1)}(z) = -\frac{i}{\pi} z^2 \log r + \frac{2i}{\pi} - \frac{z^2}{2}\left\{1 + \frac{2i}{\pi}\left[\log\left(\frac{k}{2}\right) + \gamma - 0.5\right]\right\} \tag{32}$$

This anomaly between the Green's functions in the steady case and the limiting cases does cause the convergence of the method to be frequency dependent.

To evaluate the integral in Eq. (27), a number of methods are available. For instance, when $\sqrt{\lambda_i}$ is sufficiently large, the integration can be performed efficiently by employing the fast multipole method (FMM) or the Hankel transform, based on the expansion of the Hankel function in terms of its derivatives and the Bessel functions of the first kind. In fact, the Hankel transform is equivalent to the two-dimensional Fourier transform when the input is rotationally symmetric. However, such expansions are restricted in their usefulness to far-field approximations, and our concern is more in the near field. Moreover, the set of integral equations in Eq. (27) are not merely a set of coupled Helmholtz equations.

To solve the integral Eq. (27), we express it as the sum given by

$$\begin{Bmatrix} \phi_1(x,y) \\ \phi_2(x,y) \\ \phi_3(x,y) \end{Bmatrix} = \sum_{i=1}^{3} \mathbf{R}_i \iint_S \mathbf{G}_i \mathbf{T}^{-1} \mathbf{A} \mathbf{T} \left(\frac{\partial^2}{\partial \xi^2} - \frac{\partial^2}{\partial \eta^2}\right) \begin{Bmatrix} \phi_1(\xi,\eta) \\ \phi_2(\xi,\eta) \\ \phi_3(\xi,\eta) \end{Bmatrix} \mathrm{d}\mathbf{S} + \sum_{i=1}^{3} \mathbf{R}_i \iint_S \mathbf{G}_i \mathbf{B}(\xi,\eta) \mathbf{u}(\xi,\eta)\, \mathrm{d}\mathbf{S} \tag{33}$$

and integrating the first of the two summation terms twice by parts, we have

$$\begin{Bmatrix} \phi_1(x,y) \\ \phi_2(x,y) \\ \phi_3(x,y) \end{Bmatrix} = \sum_{i=1}^{3} \mathbf{R}_i \iint_S \left(\frac{\partial^2}{\partial x^2} - \frac{\partial^2}{\partial y^2}\right) \mathbf{G}_i \mathbf{T}^{-1} \mathbf{A} \mathbf{T} \begin{Bmatrix} \phi_1(\xi,\eta) \\ \phi_2(\xi,\eta) \\ \phi_3(\xi,\eta) \end{Bmatrix} \mathrm{d}\mathbf{S} + \sum_{i=1}^{3} \mathbf{R}_i \iint_S \mathbf{G}_i \mathbf{B}(\xi,\eta) \mathbf{u}(\xi,\eta)\, \mathrm{d}\mathbf{S} \tag{34}$$

The integral Eq. (34) may be solved numerically by dividing the area of integration into panels and evaluating the integrals over the surface of integration.

It is worth noting that in the case of an isotropic plate, only ϕ_1 and ϕ_3 are required and, with the appropriate choice of the matrix $\mathbf{T}$, the integral equations reduce to the two uncoupled integral equations, which may be expressed as

$$\begin{Bmatrix} \phi_1(x,y) \\ \phi_3(x,y) \end{Bmatrix} = \sum_{i=1}^{3} \mathbf{P} \mathbf{R}_i \iint_S \mathbf{G}_i \times \mathbf{B}(\xi,\eta) \mathbf{u}(\xi,\eta)\, \mathrm{d}\mathbf{S} \tag{35}$$

where

$$\mathbf{P} = \begin{bmatrix} 1 & 0 & 0 \\ 0 & 0 & 1 \end{bmatrix} \tag{36}$$

It represents the exact solution to the problem in integral form. The solution for the transverse displacement is then recovered from Eq. (22).

The special case of the Kirchhoff theory is quite useful for purposes of comparison. In this case, the curvature-displacement relationships are

$$[\kappa_{xx} \quad \kappa_{yy} \quad \kappa_{xy}] = \left[\frac{\partial^2}{\partial x^2} \quad \frac{\partial^2}{\partial y^2} \quad \frac{\partial^2}{\partial x \partial y}\right] w(x,y) \tag{37}$$

Substituting in the moment-curvature relation and ignoring the external moment contributions,

$$\begin{Bmatrix} M_{xx} \\ M_{yy} \\ M_{xy} \end{Bmatrix} = \begin{bmatrix} D_{11} & \nu_{21} D_{11} & 0 \\ \nu_{12} D_{22} & D_{22} & 0 \\ 0 & 0 & D_{33}(1-\nu_{33})/2 \end{bmatrix} \begin{Bmatrix} \partial^2/\partial x^2 \\ \partial^2/\partial y^2 \\ 2\partial^2/\partial x \partial y \end{Bmatrix} w(x,y) \tag{38}$$

In the absence of rotary inertia, the moment equilibrium equations reduce to

$$\frac{\partial^2 M_{xx}}{\partial x^2} + 2\frac{\partial^2 M_{xy}}{\partial x \partial y} + \frac{\partial^2 M_{yy}}{\partial y^2} = q(x,y) + \rho h \omega^2 w(x,y) \tag{39}$$

We consider an orthotropic thin plate of infinite extent and assume that the external flow exerts a reactive pressure. The Kirchhoff plate equation for this case is

$$\left(a\frac{\partial^4}{\partial x^4} + 2b\frac{\partial^2}{\partial x^2}\frac{\partial^2}{\partial y^2} + c\frac{\partial^4}{\partial y^4} - \rho h \omega^2\right) w(x,y) = q(x,y) \tag{40}$$

where

$$a = D_{11}, \qquad c = D_{22},$$
$$b = D_{33} + 0.5(\nu_{21} D_{11} + \nu_{12} D_{22}) - \nu_{33} D_{33}$$

with the appropriate radiation boundary condition at infinity. Equation (40) may be written as

$$\left(b\nabla^4 + (a-b)\frac{\partial^4}{\partial x^4} + (c-b)\frac{\partial^4}{\partial y^4} - \rho h \omega^2\right) w(x,y) = q(x,y) \tag{41}$$

We note that, in principle, the solution may be expressed by employing the Fourier transform as

$$w(x,y) = \frac{1}{4\pi^2} \int_{-\infty}^{\infty} \int_{-\infty}^{\infty} [W(\alpha,\beta)]^{-1} \times \left(\int_{-\infty}^{\infty} \int_{-\infty}^{\infty} q(\xi,\eta) \exp\{-i[\alpha(x-\xi) + \beta(y-\eta)]\}\, \mathrm{d}\xi\, \mathrm{d}\eta\right) \mathrm{d}\alpha\, \mathrm{d}\beta \tag{42}$$

where

$$W(\alpha,\beta) = a\alpha^4 + 2b\alpha^2\beta^2 + c\beta^4 - \rho h\omega^2 \tag{43}$$

The governing equation for vibration of an isotropic thin plate is obtained by setting $a = b = c = D$ and is written in terms of the bi-Laplace operator as follows:

$$(D\nabla^4 - \rho h\omega^2)w(x,y) = q(x,y) \tag{44}$$

The solution may be expressed in operator form as

$$w(x,y) = \frac{1}{(\nabla^4 - \lambda^2)}\frac{q(x,y)}{D} = \frac{1}{2\lambda}\left(\frac{1}{\nabla^2 - \lambda} - \frac{1}{\nabla^2 + \lambda}\right)\frac{q(x,y)}{D} \tag{45}$$

where $\lambda^2 = \rho h\overline{\omega}^2/D$. Equations (25) and (26) are the generalization of Eq. (45).

The Green's function for the isotropic Kirchhoff plate may be expressed as

$$\mathbf{G} = -\frac{1}{2\lambda D} \times \frac{i}{4}[H_0^1(i\sqrt{\lambda}r) - H_0^1(\sqrt{\lambda}r)] \tag{46}$$

In the case when $\omega = 0$, both the roots $\pm\lambda$ reduce to zero, and we have a situation corresponding to the multiplicity of the root being equal to two.

Thus, when $\omega \neq 0$, the solution may be obtained as

$$w(x,y) = -\frac{i}{8\lambda D}\int_S\int [H_0^1(i\sqrt{\lambda}r) - H_0^1(\sqrt{\lambda}r)]q(\xi,\eta)\,\mathrm{d}\mathbf{S} \tag{47}$$

V. Application to Aeroelastic Analysis of an Aircraft Wing

The application of interest to us is the aeroelastic analysis of an aircraft wing, where the latter is modeling as an anisotropic thick wing. The unsteady aerodynamic loading on the wing due to simple harmonic motion of the wing is computed by Albano and Rodden's [15] doublet-lattice method (DLM) by using a quartic approximation for the kernel function, as defined by Vepa [16], in the context of developing finite state models of aerodynamic loads. The method, as well as certain approximations to the kernel functions, have since been validated and incorporated in several commercially available codes by Rodden et al. [17]. The method was implemented in MATLAB by the author and used to compute the aerodynamic loads at low and moderate frequencies, and by employing the piston theory limit at higher frequencies. The DLM is also an integral-equation-based approach in which a boundary integral equation relates the surface pressure loading to the upwash, which in turn is related to the displacement modes and modal velocities.

To maintain compatibility with the DLM, we divide the wing surface into trapezoidal panels and, as in the DLM, we collocate the integral Eq. (34) and evaluate the kernel functions at a set of collocation or receiving points, and at a set of integration or sending points. The collocation and integration points are assumed to be identical to those in the DLM. The solution variables in the integral Eq. (34) for the plate structural dynamics are assumed to be constants over the panels. This greatly simplifies the solution of the integral equation, although it is now not possible to numerically differentiate the discretized variables. The integral Eq. (34) is thus reduced to an algebraic equation of the form

$$\Phi = \mathbf{A}^0\Phi + \mathbf{B}^0 q \tag{48}$$

where Φ is the vector of discrete values of $\{\,\phi_1 \quad \phi_2 \quad \phi_3\,\}^T$, with the discrete values of ϕ_1 at each of the panels appearing first, followed by the discrete values of ϕ_2, and then by those of ϕ_3, and $\mathbf{A}^0$ and $\mathbf{B}^0$ are influence coefficient matrices obtained by the process of discretizing the governing matrix integral Eq. (34). In the evaluation of the influence coefficient matrices $\mathbf{A}^0$ and $\mathbf{B}^0$, two cases must be considered corresponding to the two multiplicities of the eigenvalues. Furthermore, the steady case, the low-frequency case, and the general frequency case are separately evaluated. As the coefficients are obtained by integrating the corresponding Green's functions over the area of each panel, the process is equivalent to averaging the appropriate Green's functions on the area of each panel. As each of the Green's functions is a only a function of a single variable, the averaging process is carried out equivalently by integrating with respect to this single variable of representing limits for each panel. For simplicity, it is assumed that there is no piezoelectric control loading. The solution for Φ is obtained as

$$\Phi = (\mathbf{I} - \mathbf{A}^0)^{-1}\mathbf{B}^0 q \tag{49}$$

The dynamic influence coefficient matrix relating the discrete values of the transverse displacement w to q is obtained by applying the appropriate transformation to the solution given in Eq. (49). The static influence coefficients may also be obtained in the same way by considering the case when the frequency of oscillation is set to zero. Thus, it is possible to include the effects of structural damping by introducing a suitable structural damping coefficient. Furthermore, assuming a set of response modes and applying a similarity transformation, one could construct the reduced-order modal dynamic matrix per unit area of the plate $\mathbf{D}(\omega)$, which plays the same role as $[\mathbf{K}(1 + i\omega h) - \omega^2\mathbf{M}]$ in a classical vibrating system, where $\mathbf{K}$ and $\mathbf{M}$ are the classical stiffness and mass matrices, and h is the structural damping coefficient. The damped natural frequencies, damping ratios, and normal modes of the plate may be verified by solving the eigenvalue problem defined by $[\mathbf{D}(\omega)]\mathbf{w}_i = \lambda\mathbf{w}_i$, i.e., by determining when the eigenvalues of $\mathbf{D}(\omega)$ are closest to the origin.

Thus, assuming that the corresponding set of generalized unsteady aerodynamic loads are computed by the DLM, the open-loop dynamics are written as

$$[\mathbf{D}(\omega) + q_d\mathbf{Q}(\omega, M)]\mathbf{w}_i = 0 \tag{50}$$

where $\mathbf{w}_i$ are the nondimensional modal amplitudes. The return difference equation is given by

$$[\mathbf{I} + \mathbf{GH}] = [\mathbf{I} + q_d\mathbf{D}(\omega)^{-1}\mathbf{Q}(\omega, M)] \tag{51}$$

where $\mathbf{G} = \mathbf{D}(\omega)^{-1}$ and $\mathbf{H} = q_d\mathbf{Q}(\omega, M)$. Thus, the multi-input/multi-output Nyquist plot may be obtained by computing the eigenvalues λ, defined by

$$[q_d\mathbf{Q}(\omega, M) - \lambda\mathbf{D}(\omega)]\mathbf{x} = 0 \tag{52}$$

As $\mathbf{H} = q_d\mathbf{Q}(\omega, M)$ is a complex matrix, the preceding is a complex eigenvalue problem both in the case of isotropic and anisotropic plates. To obtain the Nyquist plot corresponding to an eigenvalue, it is plotted on the complex plane as ω traverses the Nyquist contour.

We illustrate our method of aeroelastic analysis employing the preceding nonclassical Nyquist plot with a few examples. To maintain clarity, only the plot corresponding to the largest absolute eigenvalue is shown in the plot. It is natural to expect to be able to compare our results with a classical method, such as the *V-g* method, which is indeed the most commonly adopted method of analyzing flutter. All calculations of flutter speeds in the foregoing examples were verified by performing independent calculations of the flutter speeds by the *V-g* method. In the foregoing examples, the two assumed bending-torsion polynomial modes are given by

$$\phi_{i,j}\left(\frac{x}{b}, \frac{y}{s}\right) = \left(\frac{x}{b}\right)^{i-1}\left(\frac{y}{s}\right)^{j+1} \times \left[1 - 2\left(\frac{j}{j+2}\right)\frac{y}{s} + \frac{i(i+1)}{(i+2)(i+3)}\left(\frac{y}{s}\right)^2\right], \qquad i,j = 1,2$$

The same modes are assumed to evaluate the structural dynamic matrix and the aerodynamic generalized load matrix. The wing is assumed to be cantilevered, and the $y = 0$ edge is assumed to be fixed. The spanwise modal component of the assumed modes satisfy all the boundary conditions of a cantilevered beam.

Table 1 Material properties of plate models considered

Property	Units	Isotropic	Carbon-fiber	Graphite-epoxy
E_{11}	GPa	40.8	46.6	7.05
E_{22}	GPa	40.8	28.3	94.5
G_{12}	GPa	15.224	0.23	3.91
G_{31}	GPa	15.224	12.2	1.35
G_{32}	GPa	15.224	10.167	2.36
ν_{12}	——	0.34	0.45	0.0231
ν_{21}	——	0.34	0.27	0.31
ρ, actual	kg/m^3	1416.6	1416.6	1600
ρ, assumed	kg/m^3	708.3	708.3	800

As the material properties of the equivalent plate models, by and large, are closely represented by those of the principal material employed in the structure, the two anisotropic plate models and the isotropic plate model considered were based on a carbon-fiber composite laminated plate and a graphite-epoxy (T300/5208) laminated plate. The estimated and assumed material properties of these laminated plate models are presented in Table 1.

The first example considered is a 0.02-m-thick, rectangular isotropic plate model of a wing with an aspect ratio = 6, vibrating in bending and torsion at a Mach number = 0.75, and at sea level. This example was chosen because it could be solved directly by discretizing the exact integral equations representing the plate response. The rectangular half-wing was divided in six panels chordwise, whereas the semispan was divided into 36 panels. Only two parameters characterize the material properties of the isotropic plate, and these are the Young's modulus E and Poisson's ratio ν.

Although several typical values of these two parameters were considered, the Nyquist plot corresponding to just one pair of values is presented in Figs. 2 and 3. In Fig. 2, the Nyquist plot obtained by employing the Kirchhoff isotropic plate equations are compared with the corresponding Nyquist plot obtained by employing the Mindlin–Reissner isotropic plate equations. The plot shows that the effects of shear and rotary inertia are not too significant at low frequencies but very significant at high frequencies. At steady state, the error between corresponding points on the plot was less than 0.02%. The difference in the high-frequency portion of the plot illustrates the significant role played by the rotary inertia and shear component of the transverse displacement.

The convergence of the method is examined by dividing a rectangular wing of aspect ratio six into a number of panels, with the number of panels on the rectangular half-wing being 4×24, 5×30, 6×36, 7×42, or 8×48. Although 4×24 and 5×30 panels were adequate for the computation of the aerodynamic lift and moment, they were not adequate to maintain the convergence of the structural dynamic influence coefficients. As the DLM bears a close relationship to the lifting-line theories, the geometry of mesh of trapezoidal panels was chosen on the basis of aerodynamic considerations, and this required the number of panels to be chosen as $n \times 6n$, $n \times 9n$, or $n \times 12n$; i.e., the ratio of the number of semispanwise panels to the chordwise panels must lie within certain optimum limits ($>$AR and $<2 \times$ AR for rectangular half-wings) which depends on the geometry of the particular planform. Once the ratio of the number of chordwise and spanwise panels is decided, based on aerodynamic considerations, the actual numbers of panels chosen seem very much to be dictated by the need for convergence of the structural influence coefficients. Increasing the number panels increases the computation time dramatically, with marginal benefits in accuracy because of the need to keep to the aforementioned minimum ratio. Thus, an optimum of 6×36 panels were required. Figure 3 indicates that the plot corresponding to the case of 8×48 panels lies somewhere between those of 6×36 and 7×42 panels. Further computations indicated that the converged plot may lie between these two plots. For these reasons, all computations were done with 6×36 and 7×42 panels as they seem to provide upper and lower bounds for the plot. This was verified in every instance by computations with 8×48 panels. However, only the results of the preceding case are presented.

In the case of the highly anisotropic carbon-fiber composite laminated plate, with the plate thickness increased to 0.05 m thick, as in the isotropic case, but with the inertia distribution maintained the same as in the isotropic case, the associated Nyquist plot revealed a narrowband resonancelike frequency response, which is shown in Fig. 4. The frequency response seems to "lock" into a resonance peak for a small range of values of the reduced frequency k. In Fig. 4, this resonance peak manifests itself as a brief excursion across the unit circle. This type of frequency response clearly indicates that flutterlike instability is a distinct possibility when the equivalent plate thickness is reduced. Furthermore, it demonstrates the feasibility of modeling real wing structures by equivalent plate models, as all the features observed in the case of real wings are also observed in the frequency response of the equivalent plate model.

In the author's experience, for some inexplicable reason, the Nyquist plot has rarely been employed to study the stability of aeroelastic systems, although it has been used in a limited sense for controller design. In the classical Nyquist plot, the gain crossover point (i.e., when the gain exceeds unity in magnitude) and phase

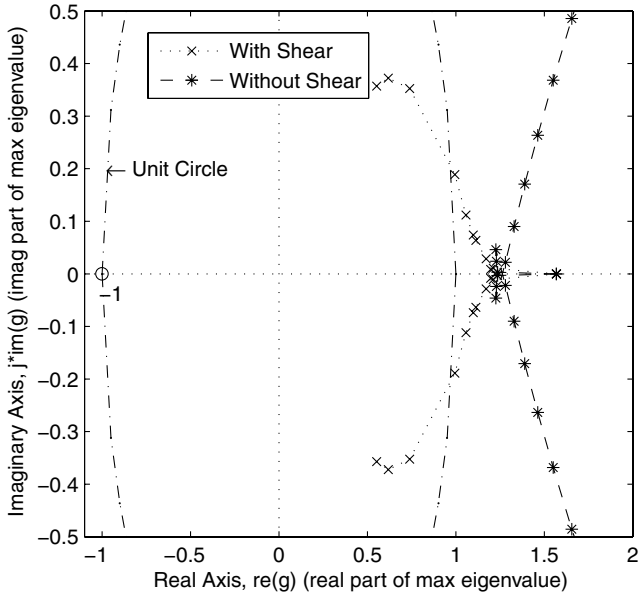

Fig. 2 Nyquist plots obtained by employing the Kirchhoff (labeled without shear) and the Reissner–Mindlin (labeled with shear) equations of the equivalent plate model of a rectangular half-wing, $M = 0.75$.

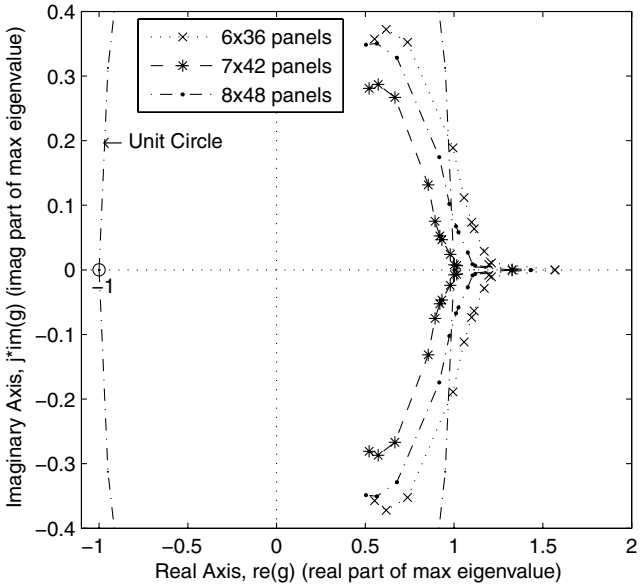

Fig. 3 Comparison of the Nyquist plots obtained for three different sets of panel discretization of the equivalent plate model of a rectangular half-wing, $M = 0.75$.

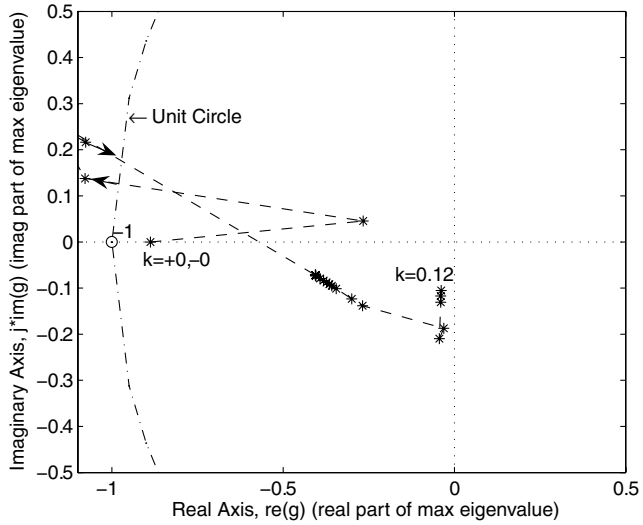

Fig. 4 Nyquist plot obtained for a 216-panel discretization of the equivalent 0.05-m-thick carbon-fiber plate model of a rectangular half-wing at $M = 0.75$.

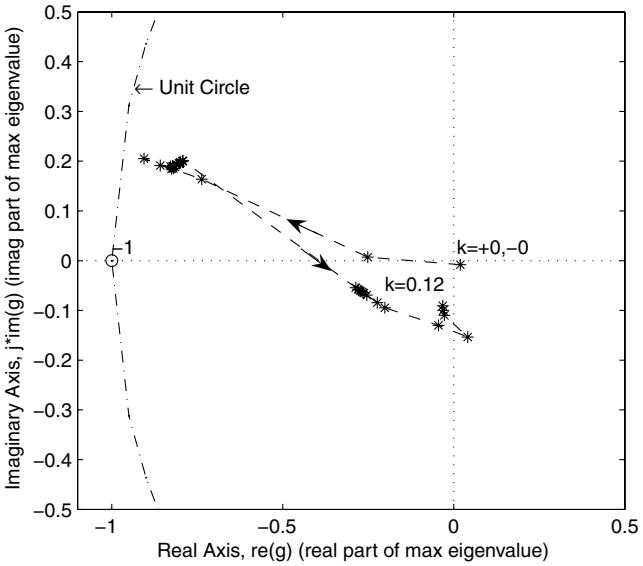

Fig. 5 Nyquist plot obtained for a 216-panel discretization of the equivalent 0.05-m-thick carbon-fiber plate model of a rectangular half-wing at $M = 0.65$.

crossover point (i.e., when phase increases from less than 180 deg to greater than 180 deg) are critical in the assessment of relative stability. The gain margin of stability is measured at the phase crossover point, and the phase margin at the gain crossover point. Moreover, when the gain crossover and the phase crossover points are relatively close to each other, it signifies that a point of neutral stability is in the vicinity of the gain crossover point. The plot in Fig. 4, which is obtained at a constant flight velocity, indicates that the classical gain margin is marginally greater than unity and the classical phase margin is negative, signifying that the plate is unstable. Aeroelastic systems are not constant gain systems, unlike classical control systems, and the gain crossover following a phase crossover indicates that there is always a lower Mach number and a higher reduced-frequency pair for which the Nyquist plot passes through the minus-one point. In a classical control system, the gain and frequency are independent of each other, whereas in an uncontrolled aeroelastic system, they are both effectively functions of a single variable, the flight velocity. Increasing (or decreasing) the flight velocity implies a rapid increase (or decrease) in the gain and a relatively slower increase (or decrease) in frequency. As the open-loop system is always unstable at Mach numbers beyond the critical

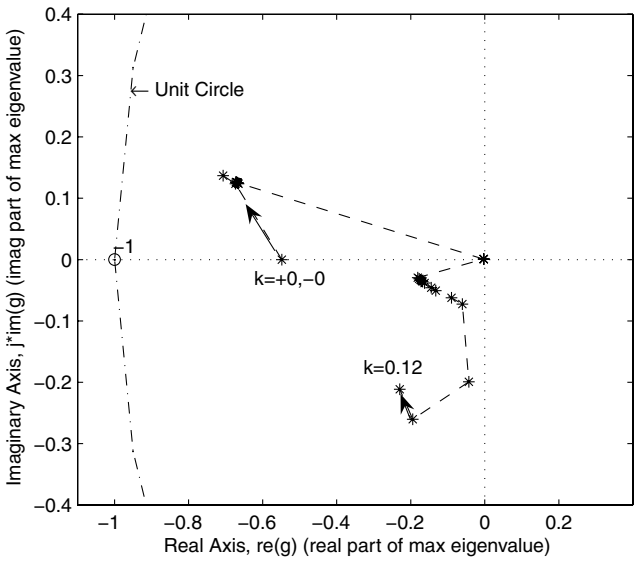

Fig. 6 Nyquist plot obtained for a 216-panel discretization of the equivalent 0.06-m-thick graphite-epoxy plate model of a rectangular half-wing, $M = 0.75$.

one at which the plot passes through the minus-one point, it follows that the gain crossover following a phase crossover implies instability. The system is only unstable beyond the critical Mach number but not below it. Plotting the frequency response in Fig. 5, at a Mach number of 0.65, reveals that the system is stable at this Mach number. A closer examination of the response reveals that when the Mach number is 0.683, the plot passes through the minus-one point. At this Mach number, the second plate resonance frequency, representing the first torsion mode, corresponds to a slightly higher reduced frequency than the flutter reduced frequency. One can expect the wing model to flutter at flight velocities beyond the one corresponding to this Mach number and is therefore unstable at the plot Mach number of 0.75 in Fig. 4. It is the behavior of the crossover points with increasing and decreasing velocity in a typical Nyquist plot that is extremely important for the assessment of relative stability. This, in fact, is completely in accordance with the interpretations of relative stability in classical controlled systems. The advantage of employing the Nyquist plot lies in the fact that one can view the entire frequency response plot and assess the relative stability, albeit at a specific Mach number.

The next example considered is the graphite-epoxy laminated plate. In this case, Young's modulus is assumed to be maximum in the spanwise direction rather than in the chordwise direction as in the previous examples. As our primary interest is in designing a stable wing, we choose a slightly higher thickness for this laminated plate model and equal to 0.06 m. The corresponding Nyquist plot is shown in Fig. 6. The plot clearly indicates that the plate model does not suffer from any instability for the system parameters under consideration. If the equivalent thickness is well below 0.06 m, we could expect the plate model to be near instability in the vicinity of the assumed flight conditions. Moreover, the directions of the principal axes of the plate, relative to the direction of the flow, are of critical importance, and this is apparent in the examples considered here.

VI. Conclusions

In this paper, we have demonstrated that by employing appropriate equivalent anisotropic plate models, it is possible to capture all the instability features of real wings. The method of analysis of the plate structure adopted here is unique and is based on a new integral equation formulation. Although the precise choice of the equivalent plate elasticity and mass parameters is still an art, the equivalent plate models can be used to effectively represent real aircraft wings. In practice, the choice of these parameters must depend on experimental data obtained from wing vibration tests and is not an easy task. Yet,

when this done, one can integrate the structural and unsteady aerodynamic modeling of any real aircraft wing without the need for extensive finite element modeling. This results in models with a few degrees of freedom without sacrificing the frequency response characteristics which are particularly vital for certain applications, such as the design of active controllers.

In this paper, we have also employed the classical Nyquist plot to assess the relative stability of the system and hence identify a critical instability point. It is argued that although the interpretations of the classical Nyquist plot to aeroelastic systems, which are not constant gain systems, are not the same as in a classical control system, it is nonetheless an extremely useful tool to gain insight into the relative stability of the system.

The main strength of the method presented in this paper lies in its application to aeroelastic analysis, particularly when the wing must be modeled as an orthotropic structure. The method could, in principle, be employed for pure vibration analysis and one is justified in naturally expecting that results of such analysis are also presented here. However, in such a case, the use of a trapezoidal mesh geometry, which is based on unsteady aerodynamic considerations, would be inappropriate and unnecessary. Furthermore, the use of the Nyquist criterion would also be unnecessary as there is no instability, and one is primarily interested in finding the natural frequencies and mode shapes of the structure. Although computations of the natural frequencies and the associated mode shapes were also performed by searching for the zeros of the dynamic matrix during the development of the method, they do not appear to fit with the theme of this paper and will be presented elsewhere in the context of the active vibration control of the structure. They are also not really necessary for implementing the method. The FEM and boundary element method (BEM) are known to be extremely successful and better for pure vibration analysis in comparison to the method presented here. In fact, in the isotropic case, the method may be considered to be equivalent to the BEM (see, for example, Wen and Aliabadi [14] for some interesting validation results). Moreover, strictly isotropic plate models rarely match the structural characteristics of real aircraft wing models employed in wing bending-torsion-type subsonic flutter analysis even when the planform is limited to a rectangle. For this reason, our focus in this paper was on the use of orthotropic plate models.

The methodology presented here can also be extended, based on the work of Murthy [3] or Phan and Reddy [4], to the case when certain nonlinearities, particularly geometric, are included in the formulation. The resulting integral equations are not linear and the extension is tedious and quite lengthy. This became apparent following the many strategies that were investigated in the course of the development of this method. However, it was found that the zig-zag theories (Carrera [8]) could quite easily be reformulated in terms of layerwise potential functions, and the present method could, in principle, be applied to laminated composite plates with layerwise orthotropic lamina, while retaining the first-order characteristic within each layer. The method of dividing the wing area into a trapezoidal mesh of panels could be applied to this case as well. The validation of such a technique would require a large number of additional computations and this was not investigated in this paper, so as to focus on the primary aspect of the paper, i.e., the coupling of the DLM with the compatible numerical evaluation of the structure's dynamic influence coefficient matrix. The layerwise first-order generalization is indeed the natural next logical step in the development of this method.

Finally, it must be stated that the method is a relatively new method and extensive validation studies are now currently being conducted, so that it can be incorporated in future commercially available codes for composite structures. A number of rules of thumb are emerging from these studies, so that the method can be applied relatively quickly to verify whether or not an aeroelastic system is stable with adequate margins within the aircraft's flight envelope. Moreover, the method may be applied to a number of other fluid-elastic interaction and instability problems, such as rectangular panels exposed only on one side to a flow and cylindrical shells with internal flow and external fluid pressure, associated with cardiovascular systems. Although the method is not capable of providing precise estimates of instability speeds without additional computations, it is proving to be extremely useful as a tool for closed-loop controller design, particularly in the context of smart structures. However, the closed-loop synthesis of the active controllers involves further considerations of the modeling aspects based on the layerwise first-order theories and will therefore be presented in an independent paper.

Acknowledgment

The author wishes to thank A. Palazotto for his constructive suggestions to improve the paper and for providing some recent references.

References

[1] Reissner, E., "Effect of Transverse Shear Deformation on the Bending of Elastic Plates," *Journal of Applied Mechanics*, Vol. 12, No. 1, 1945, pp. A-69–A-77.

[2] Mindlin, R. D., "Influence of Rotatory Inertia and Shear on Flexural Motions of Isotropic, Elastic Plates," *Journal of Applied Mechanics*, Vol. 18, 1951, pp. 31–38.

[3] Murthy, M. V. V., "Improved Transverse Shear Deformation Theory for Laminated Anisotropic Plates," NASA TP 1903, Nov. 1981.

[4] Phan, N. D., and Reddy, J. N., "Analysis of Laminated Composite Plates Using a Higher-Order Shear Deformation Theory," *International Journal for Numerical Methods in Engineering*, Vol. 21, No. 12, 1985, pp. 2201–2219.
doi:10.1002/nme.1620211207

[5] Batra, R. C., and Vidoli, S., "Higher Order Piezoelectric Plate Theory Derived from a Three-Dimensional Variational Principle," *AIAA Journal*, Vol. 40, No. 1, 2002, pp. 91–104.

[6] Demasi, L., "∞^3 Plate Theories for Thick and Thin Plates: The Generalized Unified Formulation," *Composite Structures*, 2007 (in press).
doi:10.1016/j.compstruct.2007.08.004

[7] Murakami, H., "Laminated Composite Plate Theory with Improved In-Plane Response," *Journal of Applied Mechanics*, Vol. 53, 1986, pp. 661–666.

[8] Carrera, E., "On the Use of Murakami's Zig-Zag Functions in the Modeling of Layered Plates and Shells," *Computers and Structures*, Vol. 82, Nos. 7–8, 2004, pp. 541–554.
doi:10.1016/j.compstruc.2004.02.006

[9] Carrera, E., "Historical Review of Zig-Zag Theories for Multilayered Plates and Shells," *Applied Mechanics Reviews*, Vol. 56, No. 3, May 2003, pp. 287–308.
doi:10.1115/1.1557614

[10] Kapania, R. K., and Liu, Y., "Static and Vibration Analyzes of General Wing Structures Using Equivalent-Plate Models," *AIAA Journal*, Vol. 38, No. 7, July 2000, pp. 1269–1277.

[11] Shiau, L.-C., and Wu, T.-Y., "Nonlinear Flutter of Laminated Plates with In-Plane Force and Transverse Shear Effects," *Mechanics Based Design of Structures and Machines*, Vol. 29, No. 1, April 2001, pp. 121–142.
doi:10.1081/SME-100000006

[12] Stein, M., Sydow, P. D., and Librescu, L., "Postbuckling Response of Long Thick Plates Loaded in Compression Including Higher Order Transverse Shearing Effects," NASA TM 102663, May 1990.

[13] Whitney, J. M., and Pagano, N. J., "Shear Deformation in Heterogeneous Anisotropic Plates," *Journal of Applied Mechanics*, Vol. 37, No. 4, Dec. 1970, pp. 1031–1036.

[14] Wen, P. H., and Aliabadi, M. H., "Boundary Element Frequency Domain Formulation for Dynamic Analysis of Mindlin Plates," *International Journal for Numerical Methods in Engineering*, Vol. 67, No. 11, 2006, pp. 1617–1640.
doi:10.1002/nme.1676

[15] Albano, E., and Rodden, W.P., "Doublet-Lattice Method for Calculating Lift Distributions on Oscillating Surfaces in Subsonic Flows," *AIAA Journal*, Vol. 7, Feb. 1969, pp. 279–285; Nov. 1969, p. 2192.

[16] Vepa, R., "Finite State Modeling of Aeroelastic System," NASA CR 2779, Feb. 1977.

[17] Rodden, W. P., Taylor, P. F., and McIntosh, S. C., "Further Refinement of the Subsonic Doublet Lattice Method," *Journal of Aircraft*, Vol. 35, No. 5, Sept.–Oct. 1998.

A. Palazotto
Associate Editor